Surface & Coatings Technology 311 (2017) 274–281

Contents lists available at ScienceDirect

Surface & Coatings Technology

journal homepage: www.elsevier.com/locate/surfcoat

Modulation of the morphology, microstructural and magnetic properties on electrodeposited NiFeCu alloys

R. Pereira [a], P.C. Camargo [b], A.J.A. de Oliveira [b], E.C. Pereira [a,*]

[a] Chemistry Department, Federal University of Sao Carlos, DQ-UFSCar, C.P.: 676 São Carlos, SP, Brazil
[b] Physics Department, Federal University of Sao Carlos, DF-UFSCar, CP 676 São Carlos, SP, Brazil

ARTICLE INFO

Article history:
Received 26 April 2016
Revised 20 December 2016
Accepted in revised form 21 December 2016
Available online 23 December 2016

Keywords:
Electrodeposition
NiFeCu alloys
Magnetic properties
Magnetostriction
Lattice stress

ABSTRACT

In this work, the correlations between synthesis, microstructural characteristics and magnetic properties of electrodeposited NiFeCu alloys were investigated using a factorial design procedure. The molar concentration of Ni, Fe and Cu was determined by Inductively Coupled Plasma Optical Emission Spectrometry. Field Emission Gun Scanning Electron Microscopy and Atomic Force Microscopy images ensure that all films present surface homogeneity and similar grain structure. X-ray diffraction data, analyzed using Rietveld refinement, showed that the NiFeCu alloys present face-centered cubic structure with preferential orientation in the [111] direction perpendicular to the electrode surface. It is shown that electrochemically prepared NiFeCu, can be produced to have different microstructural characteristics and composition which optimize relevant magnetic features, such as remanent (M_R) and saturation magnetization (M_S).

1. Introduction

The magnetic properties of alloys and multilayers have been investigated due to their potential application in different technological devices such as computer reader/writer heads [1], magnetic sensors [2], electromagnetic shielding [3,4], permanent magnets [5] and micro electrical mechanical system (MEMS) [6,7].

It is known from literature papers that the magnetic properties of electrodeposited alloys can be directly related not only to the composition, but also to microstructural properties, such as crystallite size, grain size, and crystal lattice deformation (strain) [8–15]. Sun et al. [16] have observed an increase in the coercivity and in the saturation magnetization for NiFe alloys associated with the increase of Fe content, leading to an anisotropic magnetic behavior. From a different point of view, Sanaty-zadeh et al. [17] have reported a decrease in the coercivity of NiFe alloys as the grain size decreases.

Different physical techniques, such as Physical Vapor Deposition (PVD), Plasma Spraying (PS) and Sputtering can be employed for film deposition. Nevertheless, wet routes like electroless and electrochemical depositions have been proven to be very efficient to obtain samples with good crystallinity, morphological quality, and high reproducibility. Besides that, electrochemical experimental parameter modulation, such as deposition potential, pH, additives, and temperature, allow the preparation of materials with a variety of morphologies. For example, the addition of saccharin to the plating solution has been used to prepare magnetic alloy with lower coercivity [18,19]. In addition, it improves the brightness of the deposit, tunes the crystal structure, decreases the grain sizes and reduces the residual stress [20]. Among its many advantages, the electrodeposition technique requires simple and inexpensive equipment, leading to a low cost of production compared to other deposition methods which require ultra-high vacuum [21–23].

The application of soft magnetic electrodeposited alloys to electronic devices have grown considerably in recent decades, for example, the use of $Ni_{80}Fe_{20}$ (Permalloy) and $Ni_{45}Fe_{55}$ alloys as reader/writer magnetic shield materials due to their high saturation magnetic flux density [24]. Besides, the addition of cooper, a nonmagnetic element, to the NiFe alloys, leads to Giant Magneto-resistance (GMR) effect. In this case, Cu plays an important role as a non-magnetic spacer in the crystal lattice of NiFe alloys and presents low lattice mismatch to the NiFe lattice common one. Specifically, for NiFeCu alloys synthesized using electrochemical methods, there are a small number of published papers [14,25–27]. Considering that electrochemical procedures have been poorly explored on preparing NiFeCu alloys, we present an experimental study on the correlation between the microstructural and morphological changes in the magnetic properties of electrodeposited thick films of NiFeCu alloys.

2. Experimental

2.1. Sample electrodeposition

The deposition bath was composed of 1.0 mol L^{-1} $NiSO_4 \cdot 7H_2O$ (Synth), 0.04 mol L^{-1} $FeSO_4$ $7H_2O$ (Sigma-Aldrich), 0.01 mol L^{-1}

* Corresponding author.
E-mail address: ernestopereira51@gmail.com (E.C. Pereira).

http://dx.doi.org/10.1016/j.surfcoat.2016.12.087
0257-8972/

$CuSO_4 \cdot 5H_2O$ (Reagen), 0.4 mol L^{-1} H_3BO_3 (Merck) and 0.01 mol L^{-1} saccharin (Synth). All solutions were prepared with water purified by a Millipore Milli-Q system (resistivity >18.2 MΩ cm) and analytical grade reagents. The pH of the solution was measured and it was equal to 3.0. Before each electrochemical synthesis, the electrolyte solution was bubbled with N_2 flux for 10 min. The N_2 flux was kept over the solution during the whole experiment. The NiFeCu alloys were electrodeposited in a three-electrode glass cell at constant temperature using a thermostatic bath (Cole Parmer, model 12104). The electrodeposition of the alloys was performed with electrodes positioned horizontally in stagnant solution. The electrochemical data were collected using an Autolab Model PGSTAT302 (Metrohm Eco Chemie) under potentiostatic control. The substrate for the depositions was polycrystalline Pt (A = 0.09 cm^2). Pt sheet (A = 2.74 cm^2) was used as an auxiliary electrode and Ag/AgCl ($KCl_{sat.}$) as the reference electrode.

2.2. Factorial design for the alloys synthesis

In the factorial design procedure the influence of all experimental variables are evaluated simultaneously. The largest advantage of this method is the evaluation of cross effects between different variables using the same set of experiments. The effects are evaluated by a matrix calculation which combines all variables at their different levels [28,29]. For the case of a combination of *n* variables at k different levels, a factorial design consists of k^n experiments. In this work 3 variables at 2 different levels were investigated leading to 8 (2^3) experiments. The parameters evaluated are deposition potential, deposition time and temperature of the plating bath.

In Table 1 the values of each experimental variable are presented. The samples were prepared and measured in duplicates and the Student's *t*-distribution with 8 degrees of freedom and 95% confidence interval was used to calculate the experimental error associated with the individual responses [28,29].

2.3. Characterization of NiFeCu alloys

The factorial design approach (Table 1) considered eight (8) samples, as well, as their duplicates. Their microstructural properties were investigated by the X-ray diffraction (XRD) using a SHIMADZU diffractometer, model XRD-6000, with CuKα radiation (λ = 1.5406 Å). A θ–2θ scan from 30° until 110° with a scan rate of 0.2°/min and step scan of 0.02° were performed at room temperature. The crystalline phases were identified using the Inorganic Crystal Structure Database (ICSD).

XDR data was analyzed by Rietveld refinement [30] using GSAS-EXPEGUI software [31]. The peak profile was fitted by a Pseudo-Voigt function of Thompson-Cox-Hasting modified by Young and Desai (pv-TCHZ) [32]. The background was corrected by an eighth-degree shifted Chebyshev polynomial function and the preferential orientation was estimated using spherical harmonics of eighth order, following a model suggested by Jarvinen [33]. In Rietveld method, the process of convergence is accompanied by χ^2, R_{WP} and RF^2 factors and a good data fit gives precise information on crystallite size, strain, preferential orientation and crystalline phases.

The film morphologies was investigated by Field Emission Gun Scanning Electron Microscopy (FEG-SEM) using a ZEISS microscope (model 105 DSM940A), with 10 keV of accelerating voltage. The Atomic Force Microscopy (AFM) mapping was performed using an Agilent series 5500 (Agilent Technologies) operating in contact mode at room temperature. A scanner of 100 μm and silicon probes (NanoSensors) with a spring constant of 10–130 N/m was used. AFM images were recorded scanning an area of 5 μm × 5 μm at a rate of 1.0 line/s. The roughness mean square (RMS) was derived from AFM micrographs using Gwyddion software [34].

The elementary chemical composition of the alloy was determined by Inductively Coupled Plasma Optical Emission Spectrometry (ICP-OES) Perkin Elmer model Optima 8300.

The magnetization was measured as a function of the applied magnetic field (M × H) performed up to 70 kOe at room temperature, using a SQUID-VSM magnetometer (MPMS®3 — QDUSA).

Table 1
Experimental parameters and levels considered in the factorial design for the electrodeposition procedure.

Variables	Levels (−)	Levels (+)	Exp.	A	B	C
E_{dep} (V)	−1.03	−1.10	E1	−	−	−
Deposition time (min)	15	40	E2	+	−	−
(C) Temperature (°C)	25	45	E3	−	+	−
			E4	+	+	−
			E5	−	−	+
			E6	+	−	+
			E7	−	+	+
			E8	+	+	+

3. Results and discussion

A set of NiFeCu alloy films were produced using experimental conditions as described in Table 1. The electrodeposition processes were performed measuring the current-time transients. Fig. 1 shows a typical current-time transient during the electrodeposition process. The current rapidly reaches a steady state in a few seconds after the process of nucleation and the growth starts, ensuring that the metal ions are being uniformly deposited in the sample [35]. The same behavior was observed for all electrodeposition conditions described in Table 1.

The compositions of Ni and Fe in the alloys obtained under different experimental conditions were evaluated using ICP-OES technique and are presented in Fig. 2a and c and Table SI-1 of the Supplementary Information. In this representation, the vertexes of the cube represent the element % composition and the axes indicate the preparation variable (applied potential, deposition time, and temperature).

The effects of the electrodeposition variables are presented by Pareto histograms. Pareto histograms are useful [36] to identify the effect of the

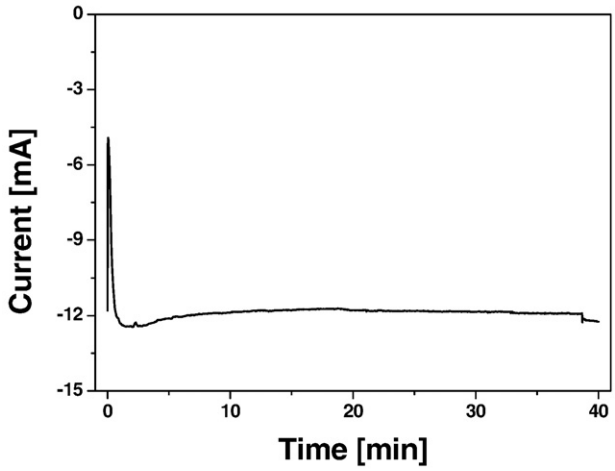

Fig. 1. Potentiostatic deposition of Experiment E3, NiFeCu film in 1 M $NiSO_4$ + 0.04 M $FeSO_4$ + 0.01 M $CuSO_4$ + 0.4 M H_3BO_3 + 0.01 M saccharin solution. E_{dep} = −1.03 V, *t* = 40 min, *T* = 25 °C.

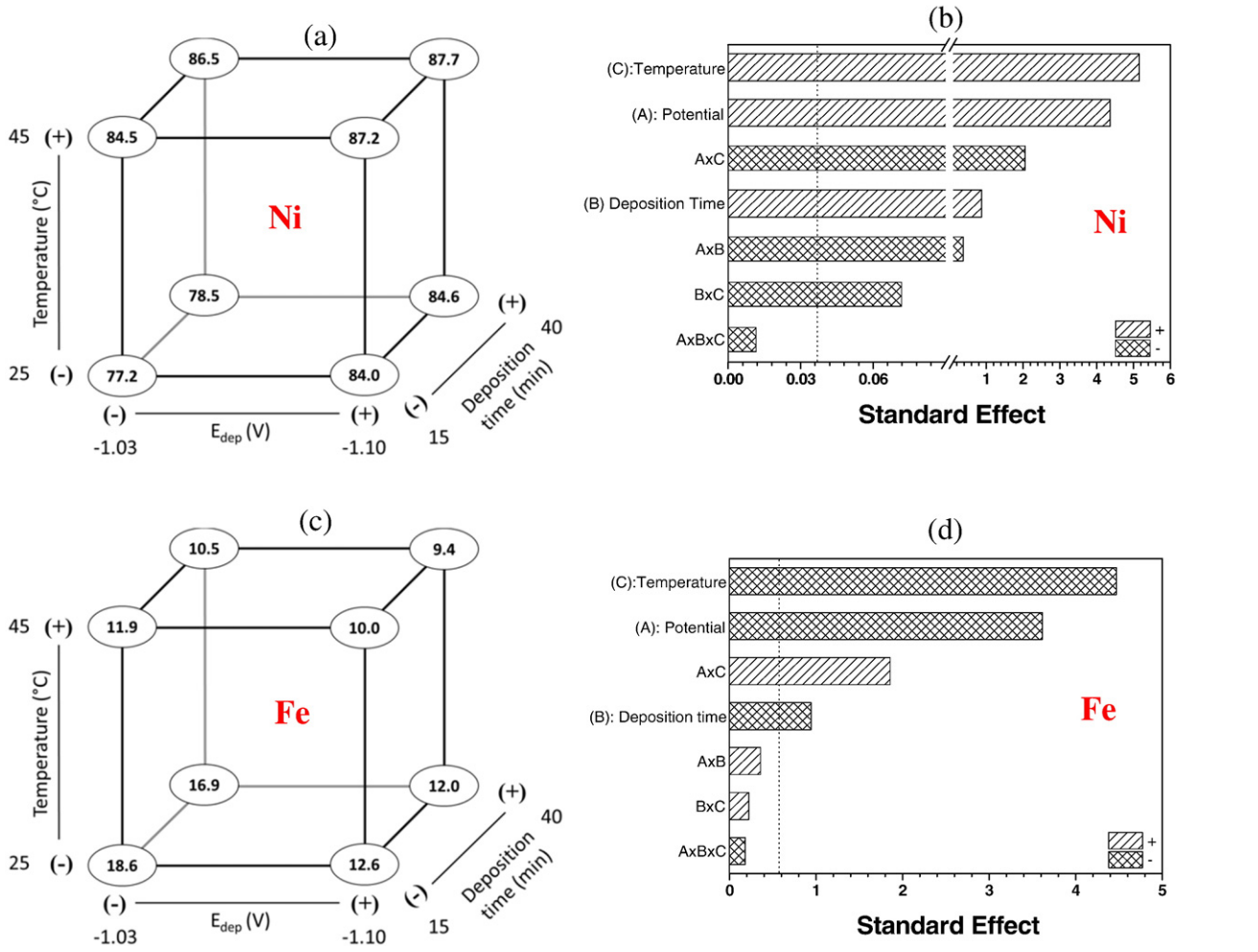

Fig. 2. Variation of % mol composition of a) Ni and c) Fe in the NiFeCu alloys. Pareto diagrams for b) Ni and d) Fe. The vertexes of the cube represent the response values and the axes indicate the parameters investigated.

variables on the responses. In Fig. 2b and d, the standardized effects are presented in a decreasing order of significance. An effect is considered statistically significant, whenever its value is equal or larger than the *t*-test critical values multiplied by the standard deviation of the effects at a 95% significance level (represented by the dotted vertical line in the chart in Fig. 2b and d [37] with eight degrees of freedom [38].

As shown in Fig. 2b and d, the temperature and the deposition potential are the parameters with the largest effect on the composition of the alloys. The standard reduction potential of Fe^{2+} ($\varphi^0_{Fe^{+2}/Fe} = -0.440$ V) is 0.183 V more negative than Ni^{2+} ($\varphi^0_{Ni^{+2}/Ni} = -0.257$ V) and 0.780 V more negative than Cu^{2+} ($\varphi^0_{Cu^{+2}/Cu} = +0.340$ V). Considering these redox potentials, it is expected that copper deposits first followed by deposition of Ni and Fe, respectively. As a consequence of the higher Ni^{+2} concentration in the electrodeposition solution the major component of the alloys is Ni (Fig. 2a) as expected. In addition, under all the experimental conditions, an increase of the Ni content reveals a competition between the kinetic reduction of nickel, iron, copper and hydrogen [39]. In our case, the displacement of the deposition potential towards more negative values and an increase in the temperature of the plating bath produce an increase of Ni concentration and a decrease Fe concentration on the alloys. This is an expected effect considering that an increase in the current density (which is a consequence of the applied potential to be more negative) results in an increase of the noble metal content in the coating [39–41].

In Fig. 3 we present surface morphologies obtained by FEG-SEM and AFM techniques of the prepared samples. FEG-SEM micrographs indicate the formation of films with similar grain structure and surface homogeneity [27] and AFM data show an increase in the grain size. This increase in the grain size could be related to the decrease in iron content in the alloy, as proposed by Sanaty-Sadeh et al. [42].

XRD profile in Fig. 4 reveals that the samples present a typical pattern of a bulk NiFeCu alloy with face-centred cubic (FCC) structure and Fm3m spatial group (ICSD 108378). The mean crystallite size, strain, lattice parameters and preferential orientation were calculated using the Rietveld refinement. This method revealed that all films of NiFeCu exhibit preferential crystallographic orientation in the [111] direction perpendicular to the film. The goodness of the data fit could be confirmed by χ^2, R_{WP} and RF^2 which are presented in Table SI-3 (Supplementary Information). All the results calculated by this method is shown in Table SI-4 (Supplementary Information).

Literature papers have reported that there is a strong correlation between changes in the chemical composition, crystallite sizes, and strain on the magnetic properties observed in many materials [8–10,13,43]. The influence of electrodeposition parameters on the magnetic properties of NiFeCu alloys was evaluated determining the magnetization as a function of the applied magnetic field ($M \times H$) at 300 K (Fig. 5). The values of the saturation magnetization (M_S) and the remanent magnetization (M_R), are shown using the geometric representation for all experimental conditions in Fig. 5b and d.

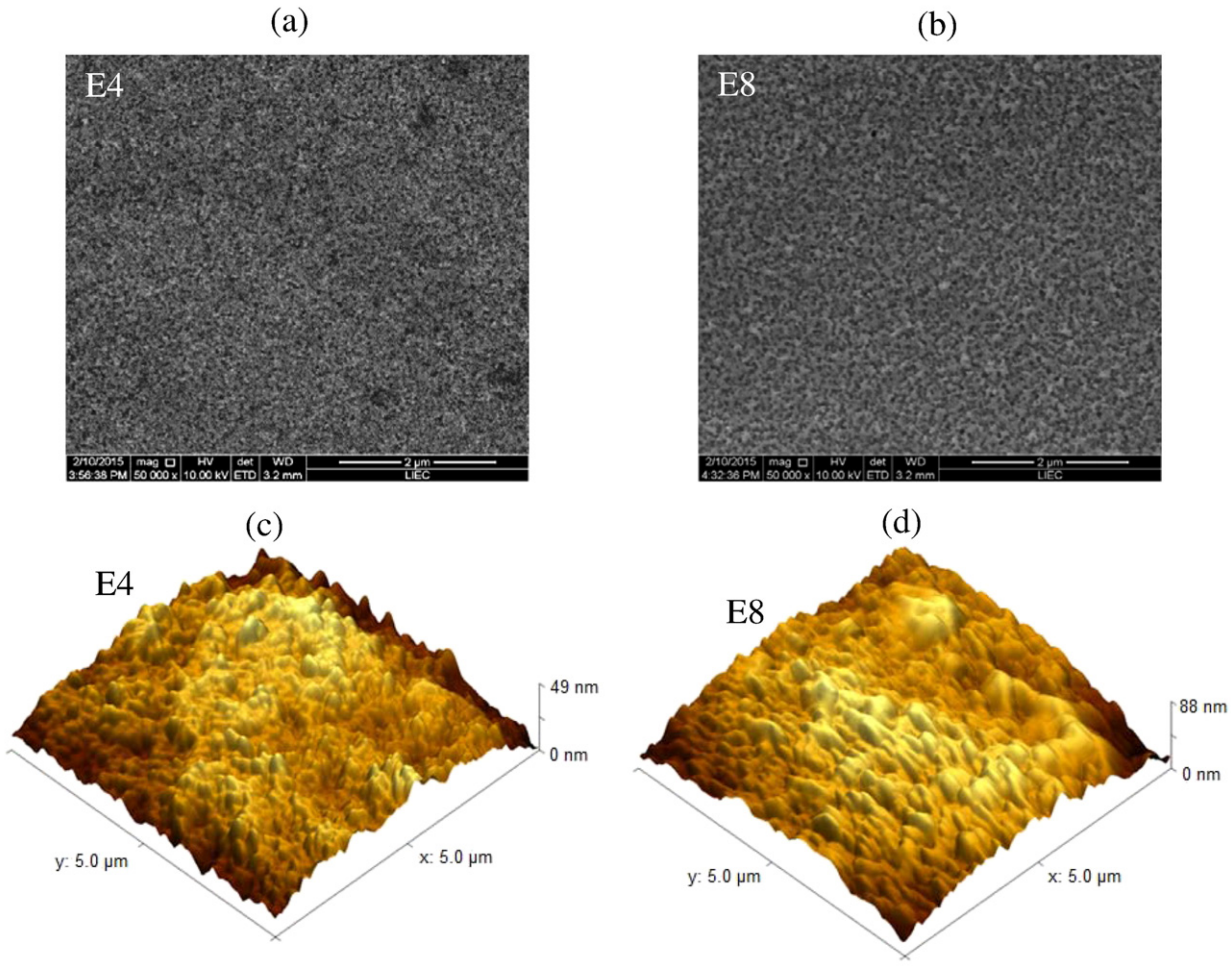

Fig. 3. In a) and b) FEG-SEM micrographs and c) and d) AFM 3-D topographic image of the sample E4 and E8. Experimental condition of sample E4: $E_{dep} = -1.10$ V, $t = 40$ min, $T = 25$ °C and E8: $E_{dep} = -1.10$ V, $t = 40$ min, $T = 45$ °C.

Fig. 5a shows an increasing M_S related to the NiFeCu alloy composition and exhibiting a maximum value of 83.4 emu g^{-1} at 300 K. Besides, NiFeCu films display a small hysteretic behavior and exhibit a low coercivity (H_C) in the range of 29 Oe to 33 Oe. These values are found to be within the limits of soft ($H_C < 12.5$ Oe) and hard ($H_C > 125$ Oe) magnetic material, being named as semi-hard ferromagnets.

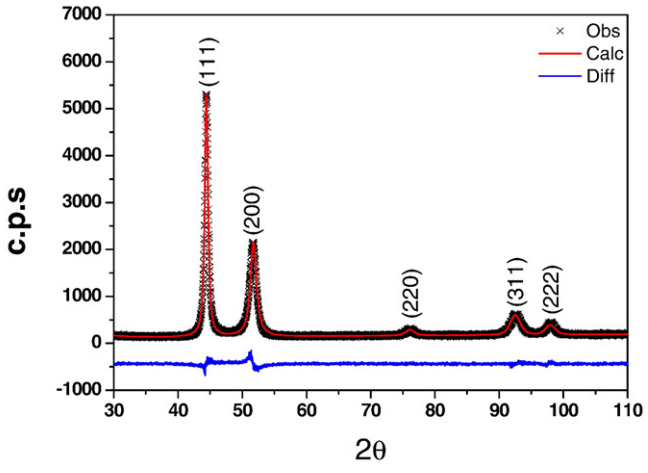

Fig. 4. Room temperature XRD pattern for sample E8 NiFeCu alloy. Preparation conditions: $E_{dep} = -1.10$ V, $t = 40$ min, and $T = 45$ °C. The black symbols (×) measured data, the red line refers to the calculated data using the Rietveld refinement method and the blue line shows the difference between the measured and calculated data.

In Fig. 5b, the geometric representation of M_S reveals that NiFeCu alloys have magnetic properties dependent on the composition and/or microstructural characteristics. The Pareto diagram (Fig. 5c and e) present the calculated standardized effect represented at Table SI-2 (Supplementary Information). The cross-effects of two-factors are also statistically significant for M_S and M_R. This means that to optimize the properties of the materials it is not enough to consider the optimization of just one variable, but it is mandatory to consider the cross effects that modulates the results [29]. Furthermore, the Pareto charts show that potential and temperature, are the most relevant variables that contributed significantly to increase M_R and M_S. This means a decrease of -16.2 ± 3.6 emu g^{-1} and -7.2 ± 2.3 emu g^{-1} for M_R and M_S, respectively, for potentials of -1.03 V to -1.10 V. Besides, when the temperature of deposition is increased, from 25 °C to 45 °C, there is a decrease of -19.6 ± 3.6 emu g^{-1} for M_R and of -3.2 ± 2.3 emu g^{-1}, for M_S. As far as the time variable is concerned it was found that M_R decreases as deposition time increases, while, H_C increases slightly (Table SI-5 — Supplementary Information). The film thickness was found proportional to the deposition time, therefore, one can associate the time of deposition with the literature data correlating the thickness of the films with M_R and H_C [44]. These results are consistent with the assumption that thicker films are likely to have a larger number of domains, resulting on an effective smaller remanence due to the domain structure [45].

These results suggest that the magnetic properties are associated with changes in the microstructure and/or composition of the alloys.

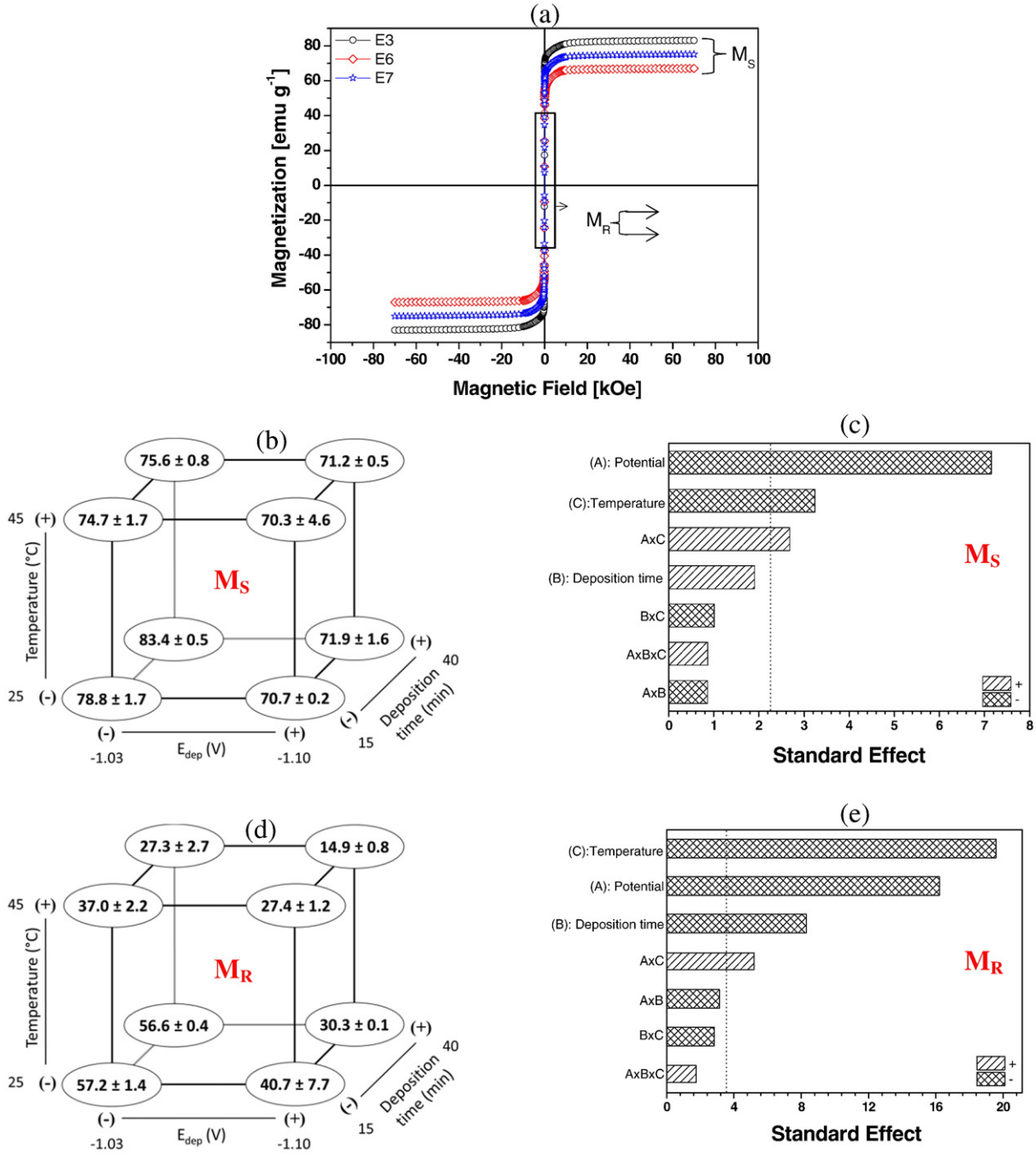

Fig. 5. In (a) magnetization as a function of the applied magnetic field at 300 K. Geometric representation and Pareto chart of saturation magnetization (M_S) b) and c) and remanent magnetization (M_R) d) and e) respectively. Experimental condition of sample E3: $E_{dep} = -1.03$ V, $t = 40$ min, $T = 25$ °C; E6: $E_{dep} = -1.10$ V, $t = 15$ min, $T = 45$ °C and $E_{dep} = -1.03$ V, $t = 40$ min, $T = 45$ °C.

In Fig.6 the dependence of M_S on the Ni and Fe content is presented. Using the red line as an eye guide, it is observed that the increase of M_S is followed by an increase of Fe and a decrease of Ni contents in the alloy. This is an expected behavior while the moment/atom for elemental Fe, $\mu_B = 2.2$ Bohr magnetron, is greater than that for Ni ($\mu_B = 0.6$) [46]. Besides, it is important to stress that M_S is an extensive characteristic of a material depending on composition, grain size and lattice strain. Therefore, it is necessary to consider the microstructural characteristics to evaluate magnetic properties.

Internal strains can influence the physical properties of almost all magnetic materials [47]. One of these effects is known as magnetostriction. A typical magnetostriction effect is caused during the deposition process and this effect is revealed in M × H curves [46]. For NiFe alloys this effect was already observed [48] by Butta et al. In our case, the calculated strain, calculated from XRD data Rietveld refinement, ranged from 2.01% to 3.05% (Table SI-4 — Supplementary Information). In Fig. 7 the square of the magnetization normalized by the saturation magnetization, $(M/M_S)^2$, is presented as a function of the applied magnetic field, for different NiFeCu alloys at 300 K. As can be observed in Fig. 7, the curves quickly increase in the region of low fields and then slowly achieve the saturation. The difference between the curves in the low field region arises due to domain walls movement

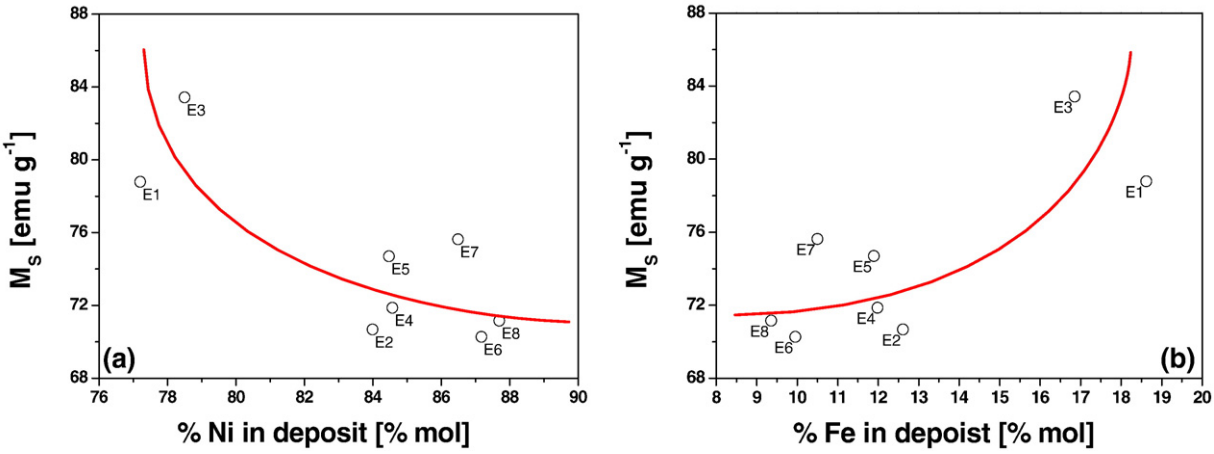

Fig. 6. Saturation magnetization (M_S) of NiFeCu alloys. In a) % Ni and b) % Fe deposited. The red line is a guideline.

[49] and to different strains generated during the electrodeposition process, which give origin to the magnetostriction effect. The magnetostriction effect is directly proportional to $(M/M_S)^2$ [47]. The arrow in Fig. 7 shows a decrease in $(M/M_S)^2$ associated with the decreasing lattice strain.

Several published results describe that the remanent magnetization is strongly dependent on the crystallite size (D) [50–55]. In Fig. 8a $M_R \times D$ data is presented, showing an increase in the remanent magnetization for D such as $5.4 \le D \le 6.1$ at 25 °C and to $6.6 \le D \le 7.7$ at 45 °C. The same pattern is observed when the remanent magnetization is plotted as a function of the Fe content as shown by a linear dependence between M_R on %Fe (Fig. 8b). The remanent magnetization as a function of %Ni follows the expected linear decrease due to the decreasing effective moment/atom.

In conclusion, the employed technique was effective for obtaining NiFeCu films with the desired microstructural characteristics and composition to optimize magnetic relevant features, such as remanent (M_R) and saturation magnetization (M_S).

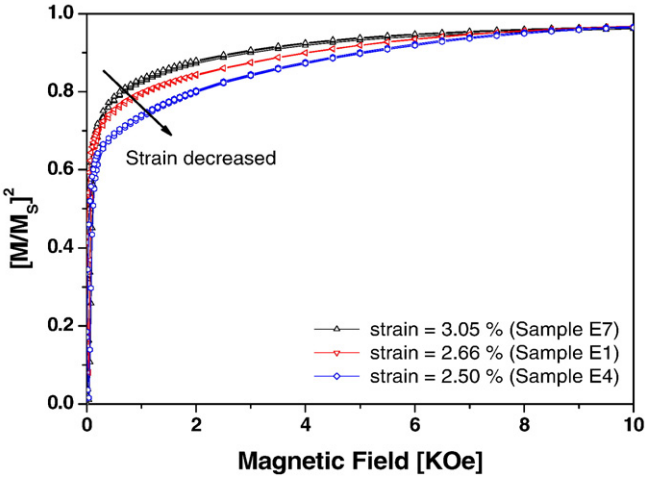

Fig. 7. Magnetostriction effect $(M/MS)^2$ as a function of applied magnetic field for NiFeCu alloys at room temperature. The arrow indicates that a reduction in the lattice strain is associated to a reduction in the magnetostriction effect. Preparation conditions: E1: $E_{dep} = -1.03$ V, $t = 15$ min, $T = 25$ °C; E4: $E_{dep} = -1.10$ V, $t = 40$ min, $T = 25$ °C and E7: $E_{dep} = -1.03$ V, $t = 40$ min, $T = 45$ °C.

4. Conclusions

In this work, we have shown that using standard electrochemical variables it is possible to control the magnetic properties aiming at different applications. The modification of electrodeposition parameters using factorial design allowed us to obtain significant changes in the magnetic properties of the alloys and to quantify the effects of each variable, as well as, the existence of cross effect as clearly seen in Pareto diagrams. The potential of deposition and temperature of the plating bath causes consistent changes of composition, morphology, microstructure and magnetic properties of the alloys.

All electrodeposited NiFeCu alloys exhibit face-centred cubic (FCC) crystalline structure with preferential orientation in the [111] direction. Morphology analysis indicates that NiFeCu alloy films have similar grainy structure and surface homogeneity. AFM data shows that increasing the temperature of the plating bath increases grain size.

The study of the correlation between the magnetic behavior and the microstructural characteristics show that an increase in magnetostriction effect is associated with an increase in the lattice strain calculated by XRD Rietveld refinement. In addition, the magnetic behavior of the films shows that the remanent (M_R) and saturation magnetization (M_S) depends strongly on the Ni and Fe contents, on the lattice stress and on the crystallite size.

The geometric representation and Pareto chart summarize the general conclusion that the external variables, temperature, potential and deposition time, can be used to prepare NiFeCu alloys controlling standard electrochemical variables.

It is shown that electrochemically prepared NiFeCu films, can be produced to have different microstructural characteristics and composition to optimize magnetic relevant features, such as remanent (M_R) and saturation magnetization (M_S).

Acknowledgments

The authors thank to FAPESP (2012/22934-2 and 2013/07296-2), CNPq and CAPES for financial support.

Appendix A. Supplementary data

Supplementary data to this article can be found online at http://dx.doi.org/10.1016/j.surfcoat.2016.12.087.

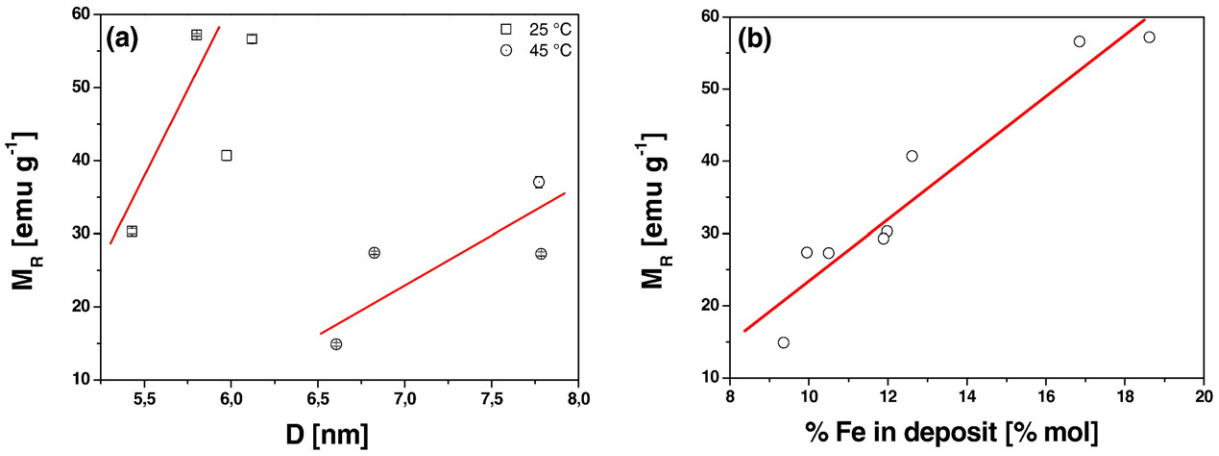

Fig. 8. Dependence of remanent magnetization (M_R) of NiFeCu alloy: a) crystallite size and b) % Fe in the deposit. The red line is a guideline.

References

[1] K. Nikolaev, P. Kolbo, T. Pokhil, X. Peng, Y. Chen, T. Ambrose, et al., "All-Heusler alloy" current-perpendicular-to-plane giant magnetoresistance, Appl. Phys. Lett. 94 (2009) 222501.

[2] A. Zhukov, M. Churyukanova, S. Kaloshkin, V. Semenkova, S. Gudoshnikov, M. Ipatov, et al., Effect of annealing on magnetic properties and magnetostriction coefficient of Fe–Ni-based amorphous microwires, J. Alloys Compd. 651 (2015) 718–723.

[3] N.N. Lu, X.J. Wang, L.L. Meng, C. Ding, W.Q. Liu, H.L. Shi, et al., Electromagnetic interference shielding effectiveness of magnesium alloy-fly ash composites, J. Alloys Compd. 650 (2015) 871–877.

[4] K. Song, F.S. Pan, X.H. Chen, Z.H. Zhang, A.T. Tang, J. She, et al., Effect of texture on the electromagnetic shielding property of magnesium alloy, Mater. Lett. 157 (2015) 73–76.

[5] C. Bran, E.M. Palmero, R.P. del Real, M. Vazquez, CoFeCu electroplated nanowire arrays: role of composition and annealing on structure and magnetic properties, Phys. Status Solidi 211 (2014) 1076–1082.

[6] H.S. Akkera, I. Singh, D. Kaur, Martensitic phase transformation of magnetron sputtered nanostructured Ni–Mn–In ferromagnetic shape memory alloy thin films, J. Alloys Compd. 642 (2015) 53–62.

[7] J. Xu, L. Shi, C. Wang, D. Shan, B. Guo, Micro hot embossing of micro-array channels in ultrafine-grained pure aluminum using a silicon die, J. Mater. Process. Technol. 225 (2015) 375–384.

[8] A. Kolano-Burian, R. Kolano, Ł. Hawełek, J. Szynowski, P. Włodarczyk, Correlation between nanocrystalline and magnetic structure of Co-based alloys with the induced transverse magnetic anisotropy, J. Appl. Phys. 115 (2014), 183904. .

[9] P. Gorria, V.M. Prida, M. Tejedor, B. Hernando, M.L. Sánchez, Correlation between structure, magnetic properties and MI effect during the nanocrystallisation process of FINEMET type alloys, Phys. B Condens. Matter 299 (2001) 215–224.

[10] M.S. Khatri, H. Schlörb, S. Fähler, L. Schultz, Correlation of crystallographic structure and magnetic properties of electrodeposited Co-rich Co-Pt films, Phys. Status Solidi 208 (2011) 104–108.

[11] H. Ehrenberg, I. Dincer, A. Elmali, Y. Elerman, H. Fuess, Magnetic and crystal structure correlations in $PrMn_{1.5}Co_{0.5}Ge_2$: a synchrotron diffraction study, Solid State Commun. 124 (2002) 429–432.

[12] R.D. Noce, O.D.M. Gomes, S.D. De Magalhães, W. Wolf, R.B. Guimarães, A.C. De Castro, et al., Magnetic properties of Fe-Cu alloys prepared by pulsed electrodeposition, J. Appl. Phys. 106 (2009) 93907.

[13] B.N. Mondal, A. Basumallick, P.P. Chattopadhyay, Correlation of microstructure and magnetic properties in Cu-Co-Ni alloys, Mater. Sci. Eng., B 166 (2010) 174–179.

[14] S. Esmaili, M.E. Bahrololoom, L. Peter, Magnetoresistance of electrodeposited NiFeCu alloys, Thin Solid Films 520 (2012) 2190–2194.

[15] C.Z. Wang, G.W. Meng, Q.Q. Fang, X.S. Peng, Y.W. Wang, Q. Fang, et al., Structure and magnetic property of Ni-Cu alloy nanowires electrodeposited into the pores of anodic alumina membranes, J. Phys. D. Appl. Phys. 35 (2002) 738–741.

[16] Y. Sun, Q. Liang, Y. Zhang, Y. Tian, Y. Liu, F. Li, et al., Controlled synthesis of magnetic Ni-Fe alloy with various morphologies by hydrothermal approach, J. Magn. Magn. Mater. 332 (2013) 85–88.

[17] A. Sanaty-Zadeh, K. Raeissi, A. Saidi, Magnetic properties of nanocrystalline Fe–Ni alloys synthesized by direct and pulse electrodeposition, Int. J. Mod. Phys. B 25 (2011) 2031.

[18] T. Osaka, T. Yokoshima, D. Shiga, K. Imai, K. Takashima, A high moment CoFe soft magnetic thin film prepared by electrodeposition, Electrochem. Solid-State Lett. 6 (2003) C53–C55.

[19] I. Tabakovic, S. Riemer, V. Inturi, P. Jallen, A. Thayer, Organic additives in the electrochemical preparation of soft magnetic CoNiFe films, J. Electrochem. Soc. 147 (2000) 219–226.

[20] J. George, J. Rantschler, S.-E. Bae, D. Litvinov, S.R. Brankovic, Sulfur and saccharin incorporation into electrodeposited CoFe alloys: consequences for magnetic and corrosion properties, J. Electrochem. Soc. 155 (2008) D589–D594.

[21] J. Yang, S. Huang, Z. Wang, Y. Hou, Y. Shi, J. Zhang, et al., Synthesis of copper nitride films doped with Fe, Co, or Ni by reactive magnetron sputtering, J. Vac. Sci. Technol. A 32 (2014) 051510.

[22] L. Lai, W. Zeng, X. Fu, R. Sun, R. Du, Optimization of sputtering parameters for Ni-Cr alloy deposition on copper foil as embedded thin film resistor, Surf. Coat. Technol. 218 (2013) 80–86.

[23] B. Meng, Y. Sun, X.D. He, J.H. Peng, Fabrication and characterization of Ni-YSZ anode functional coatings by electron beam physical vapor deposition, Thin Solid Films 517 (2009) 4975–4978.

[24] E.I. Cooper, C. Bonhote, J. Heidmann, Y. Hsu, P. Kern, J.W. Lam, et al., Recent developments in high-moment electroplated materials for recording heads, IBM J. Res. Dev. 49 (2005) 103–126.

[25] M.C. Baykul, U. Sarac, M. Alper, Surface morphology, structural and magnetic properties of electrodeposited NiFeCu/Cu films, J. Supercond. Nov. Magn. 25 (2012) 2585–2589.

[26] S. Kang, M. Takeda, Z. Hiroi, G.W. Kim, C.G. Lee, B.H. Koo, Magnetic and magnetoresistive properties related to microstructure in Cu_{75}–Fe_5–Ni_{20} alloys, J. Phys. D. Appl. Phys. 43 (2010) 415001.

[27] H. Kuru, H. Kockar, M. Alper, Electrodeposited NiFeCu/Cu multilayers: effect of Fe ion concentration on properties, J. Magn. Magn. Mater. 373 (2015) 135–139.

[28] R.G. Brereton, Chemometrics — Data Analysis for the Laboratory and Chemical Plant, John Wiley, England, 2003 15–84.

[29] R.E. Bruns, I.S. Scarminio, B.B. Neto, Statical Design — Chemometrics, Elsevier Science, Amsterdan, 2006 105–112.

[30] H.M. Rietveld, Line profiles of neutron powder-diffraction peaks for structure refinement, Acta Crystallogr. 22 (1967) 151–152.

[31] B.H. Toby, EXPGUI, a graphical user interface for GSAS, J. Appl. Crystallogr. 34 (2001) 210–213.

[32] R.A. Young, P. Desai, Crystallite size and microstrain indicators in Rietveld refinement, Arch. Nauki Mater. (Arch. Mater. Sci.), 10 (1989) 71–90.

[33] M. Jarvinen, Application of symmetrized harmonics expansion to correction of the preferred orientation effect, J. Appl. Crystallogr. 26 (1993) 525–531.

[34] D. Nečas, P. Klapetek, Gwyddion: an open-source software for SPM data analysis, Cent. Eur. J. Phys. 10 (2012) 181–188.

[35] A.J. Bard, L.R. Faulkner, Electrochemical Methods — Fundamentals and Applications, Second ed., New York, 2001 209–210.

[36] D.L. Massart, B.G.M. Vandeginte, L.M.C. Buydens, S. de Jong, P.J. Lewi, J. Smeyers-Verbek, Handbook of Chemometrics and Qualimetrics, Part A, Elsevier, Amstermdam, 2003 21–150.

[37] G.E.P. Box, W.G. Hunter, J.S. Hunter, Statistic for Experiments: An Introduction to Design, Data Analysis, and Model Building, John Wiley, New York, 1978 19–125.

[38] W. Hardle, L. Simar, Applied Multivariate Statistical Analysis, third ed. Springer, Berlin and Louvain-la-Neuve, 2003 55–181.

[39] P. Fricoteaux, C. Rousse, Influence of substrate, pH and magnetic field onto composition and current efficiency of electrodeposited Ni–Fe alloys, J. Electroanal. Chem. 612 (2008) 9–14.

[40] I. Rodriguez-Torres, G. Valentin, F. Lapicque, Electrodeposition of zinc-nickel alloys from ammonia-containing baths, J. Appl. Electrochem. 29 (1999) 1035–1044.

[41] S.S.A. ElRehim, E.E. Fouad, S.M.A. ElWahab, H.H. Hassan, Electroplating of zinc-nickel binary alloys from acetate baths, Electrochim. Acta 41 (1996) 1413–1418.

[42] A. Sanaty-Zadeh, K. Raeissi, A. Saidi, Properties of nanocrystalline iron–nickel alloys fabricated by galvanostatic electrodeposition, J. Alloys Compd. 485 (2009) 402–407.

[43] C. Suryanarayana, Nanocrystalline materials, Int. Mater. Rev. 40 (1995) 41–64.

[44] A. Karpuz, H. Kockar, M. Alper, Applied surface science properties of electrodeposited Co–Mn films: influence of deposition parameters, Appl. Surf. Sci. 358 (2015) 605–611.

[45] H. Kockar, M. Alper, H. Kuru, T. Meydan, Magnetic anisotropy and its thickness dependence for NiFe alloy films electrodeposited on polycrystalline Cu substrates, J. Magn. Magn. Mater. 304 (2006) E736–E738.

[46] R.M. Bozorth, Ferromagnetism, John Wiley, New Jersey, 2003 15–85.

[47] B.D. Cullity, C.D. Graham, Introduction to Magnetic Materials, John Wiley & Sons, Inc., New Jersey, 2008 197–272.
[48] M. Butta, M. Janosek, P. Ripka, L. Kraus, R. El Kammouni, Influence of magnetostriction of NiFe electroplated film on the noise of fluxgate, IEEE Trans. Magn. 50 (2014) 2–5.
[49] S. Blundell, Magnetism in Condensed Matter, Oxford Uni, New York, 2001 128–135.
[50] Y. Honda, Y. Hirayama, K. Ito, M. Futamoto, Microscopic magnetization structures and noise in single-layer perpendicular thin film media, IEEE Trans. Magn. 34 (1998) 1633–1635, http://dx.doi.org/10.1109/20.706639.
[51] H.M.I. Abdallah, T. Moyo, N. Ngema, The effect of temperature on the structure and magnetic properties of $Co_{0.5}Ni_{0.5}Fe_2O_4$ spinel nanoferrite, J. Magn. Magn. Mater. 394 (2015) 223–228.
[52] M.Y. Rafique, L. Pan, W.S. Khan, M.Z. Iqbal, H. Qiu, M.H. Farooq, et al., Controlled synthesis, phase formation, growth mechanism, and magnetic properties of 3-D CoNi alloy microstructures composed of nanorods 3, CrystEngComm 15 (2013) 5314–5325.
[53] M.Y. Rafique, L. Pan, M. Zubair Iqbal, Q. Javed, H. Qiu, M.H. Farooq, et al., 3-D flower like FeCo alloy nanostructures assembled with nanotriangular prism: facile synthesis, magnetic properties, and effect of NaOH on its formation, J. Alloys Compd. 550 (2013) 423–430.
[54] C.V. Reddy, C. Byon, B. Narendra, D. Baskar, G. Srinivas, J. Shim, et al., Investigation of structural, thermal and magnetic properties of cadmium substituted cobalt ferrite nanoparticles, Superlattice. Microst. 82 (2015) 165–173.
[55] Z.Q. Jin, N.N. Thadhani, M. McGill, J. Li, Y. Ding, Z.L. Wang, et al., Grain size dependence of magnetic properties in shock synthesized bulk $Pr_2Fe_{14}B/\alpha$-Fe nanocomposites, J. Appl. Electrochem. 96 (2004) 3452–3457.